Cell Reports
Physical Science

CellPress
OPEN ACCESS

Report

Full-Color Spectrum Coverage by High-Color-Purity Perovskite Nanocrystal Light-Emitting Diodes

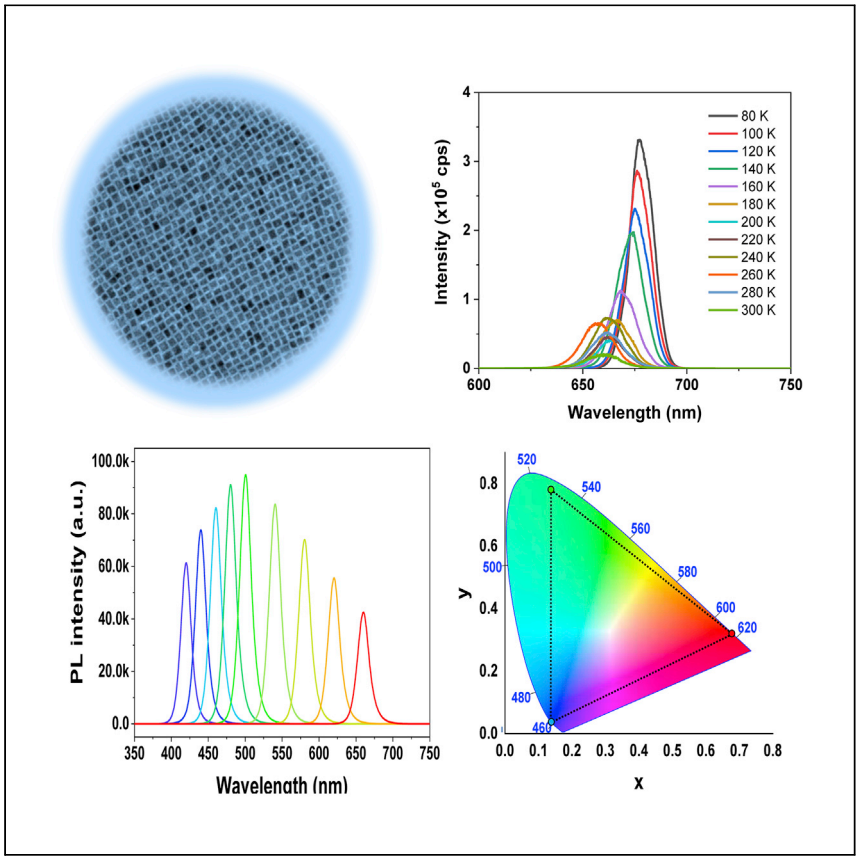

Heo et al. report that hydrogen halide (HX; X = Cl, Br, and I)-mediated synthesis promotes the reaction for the formation of CsX and subsequent anion exchange. This forms compositionally uniform perovskite nanocrystals exhibiting single emission peaks at low temperature.

Jin Hyuck Heo, Jin Kyoung Park, Sang Hyuk Im

imromy@korea.ac.kr

HIGHLIGHTS

HX-mediated method produces compositionally uniform perovskite nanocrystals

Perovskite nanocrystals do not have metallic Pb impurities

Full-color perovskite nanocrystals exhibit high color purity

Heo et al., Cell Reports Physical Science *1*, 100177
September 23, 2020 © 2020 The Authors.
https://doi.org/10.1016/j.xcrp.2020.100177

Cell Reports
Physical Science

CellPress
OPEN ACCESS

Report

Full-Color Spectrum Coverage by High-Color-Purity Perovskite Nanocrystal Light-Emitting Diodes

Jin Hyuck Heo,[1,2] Jin Kyoung Park,[1,2] and Sang Hyuk Im[1,3,*]

SUMMARY

Although many synthetic methods such as hot injection and anionic exchange can produce full-color perovskite nanocrystals (PNCs), their emission spectra are broadened by compositional non-uniformity. Here, we propose the synthetic method, hydrogen halide (HX; X = Cl, Br, and I)-mediated uniform halide anion exchange at mild temperatures, for high color-purity PNCs emitters across the full-color spectrum. The HX-mediated exchange reaction produces high-purity PNCs without metallic Pb impurities due to the use of volatile HX as the X source. The blue, green, and red PNCs show narrow emission spectra, with 16, 18, and 18.5 nm of full width at half-maximum, respectively. The red PNC emitter synthesized by the HX-mediated method has a single photoluminescent (PL) peak, with a narrow emission spectrum at low temperature due to compositional uniformity, whereas the PNCs produced by other methods have multiple PL peaks. Accordingly, the red/green/blue electroluminescent devices also have narrow emission spectra.

INTRODUCTION

To date, perovskite light-emitting diodes (PLEDs) have been considered next-generation light emitters replacing organic LEDs and quantum dot LEDs because of their unique properties such as high photoluminescent quantum yield (PLQY), convenient emission color control, high color purity, and solution processability.[1–7] Because of the small exciton binding energies of bulk perovskite materials, the perovskite materials should physically confine the excitons within nanosized perovskite crystal grains.[8–10] Therefore, perovskite nanocrystals (PNCs) such as $CsPbX_3$ (X = Cl, Br, I, and their mixtures) are ideal for demonstrating full-color PLEDs with high color purity.[11]

To demonstrate full color for displays with PNCs, halide ions such as Cl and I should be exchanged from $CsPbBr_3$ PNCs in solution chemistry. However, it is problematic that the emission spectrum of full width at half-maximum (FWHM) is broadened by non-uniform halide mixing or halide anion exchange.[12–16] Here, we synthesized blue, green, and red $CsPbX_3$ PNCs emitters with <20 nm of FWHMs by hydrogen halide (HX)-mediated uniform anionic exchange at mild temperature and demonstrated high-color-purity PNC-based LEDs emitting red, green, and blue colors.

RESULTS

HX-Mediated Anionic Exchange Reaction for $CsPbX_3$ PNCs

Figure 1A is a schematic illustration of reaction procedures and related chemical reactions for the synthesis of high-color-purity $CsPbX_3$ PNCs. For a typical synthesis of

[1]Department of Chemical and Biological Engineering, Korea University, 145 Anam-ro, Seongbuk-gu, Seoul 17104, Republic of Korea

[2]These authors contributed equally

[3]Lead Contact

*Correspondence: imromy@korea.ac.kr

https://doi.org/10.1016/j.xcrp.2020.100177

This is an open access article under the CC BY license (http://creativecommons.org/licenses/by/4.0/).

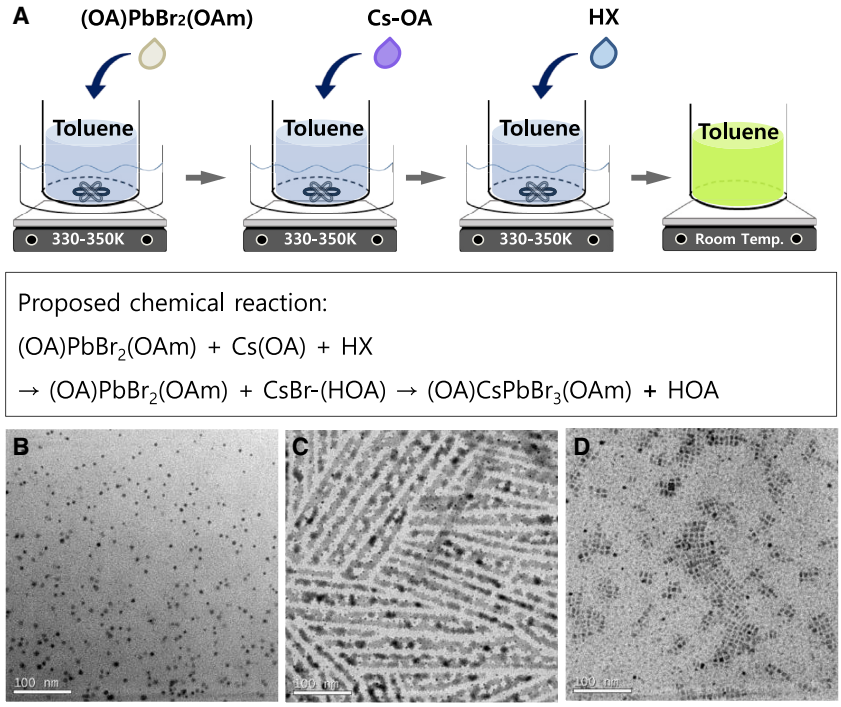

Figure 1. Chemical Reaction Scheme for the Synthesis of High-Color-Purity $CsPbX_3$ PNCs

(A) Schematic illustration of reaction procedure and related chemical reactions.

(B–D) TEM images of each reaction step: (B) (OA)$PbBr_2$(OAm) solution, (C) (OA)$PbBr_2$(OAm) + CsOA, and (D) (OA)$PbBr_2$(OAm) + CsOA + HBr.

the $CsPbBr_3$ green PNC emitter, a cesium oleate (Cs(OA)) and a $PbBr_2$-ligand ((OA)$PbBr_2$(OAm)) solution was prepared by reacting Cs carbonate with oleic acid and reacting $PbBr_2$ with oleylamine (OAm) and OA, respectively. Both solutions were stirred on a hot plate pre-set to 80°C for ~40 min until the reactant chemicals were completely dissolved. Then, a vial containing toluene (TOL) was immersed in an oil bath at ~60°C. The (OA)$PbBr_2$(OAm) solution, the Cs(OA) solution, and the HBr solution was dropped into the vial in order. On dropping the HBr solution, the mixed solution began to turn from transparent to yellow-green and then to fluorescent green within 2 min. For a sufficient reaction, the mixture was stirred for ~10 min more and taken out at room temperature. Here, we provide the deficient halide (Br) source from HBr so that impurities do not remain in the reaction batch because the excess HBr will have evaporated.

Figures 1B–1D are the transmission electron microscopy (TEM) images of each reaction step, showing what is happening in each step. Figure 1B confirms the formation of very tiny $PbBr_2$ nanocrystals by mixing $PbBr_2$ and OAm/OA ligands. Figure 1C displays a wire-like morphology, which is composed of a mixture of tiny $PbBr_2$ nanocrystals and Cs(OA) because the molecular structure of Cs(OA) is similar to the surfactant. Figure 1D clearly indicates that the HBr triggers the reactions and produces the cube-shaped $CsPbBr_3$ PNCs because the HBr reacts with Cs(OA) immediately and produces CsBr, as shown in Figure S1.

Figures 2A–2C are the photoluminescence (PL) spectra evolution with reaction time for the synthesis of $CsPbBr_3$ PNCs to check the effect of the ratio of HBr to $PbBr_2$ in the reaction. We measured the *in situ* PL spectra every 2 s after the injection of the HBr solution, as shown in Figure 2D. As the molar ratio of HBr:$PbBr_2$ increases, the

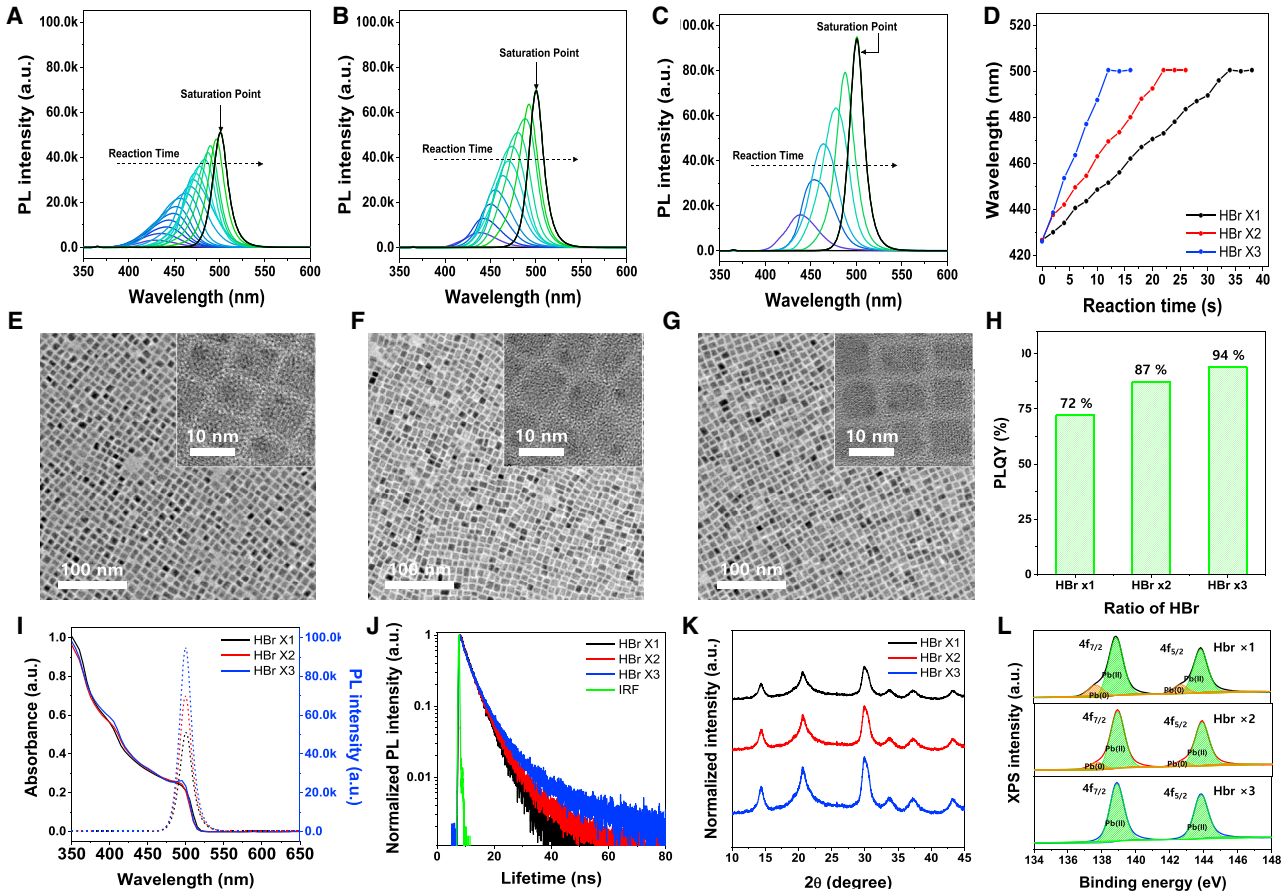

Figure 2. ***In Situ*** **Photoluminescence Spectra and Characterization of $CsPbBr_3$ PNCs**

(A–D) PL spectra evolution with time according to the ratio HBr:$PbBr_2$: (A) 1:1, (B) 2:1, (C) 3:1, and (D) plots of the PL maximum wavelength over reaction time.

(E–G) TEM images of produced $CsPbBr_3$ PNCs by HBr:$PbBr_2$ of 1:1 (E), 2:1 (F), and 3:1 (G); insets, high-resolution TEM.

(H and I) Characterization of corresponding PNCs: (H) PL quantum yield (PLQY) and (I) UV-visible absorption and static PL spectra.

(J) Transient PL spectra.

(K) X-ray diffraction (XRD) patterns.

(L) X-ray photoelectron spectroscopy (XPS) spectra.

saturation time of the PL spectrum shift was gradually reduced to 34 s for the 1:1 (HBr × 1) sample, 22 s for the 2:1 (HBr × 2) sample, and 12 s for the 3:1 (HBr × 3) sample. The accelerated reaction rate may be attributed to the increased reaction rate between Cs(OA) and HBr. Irrespective of the ratio of HBr:$PbBr_2$, the saturated PL peak positions were similar because the excess HBr will have evaporated, except for the promotion of the forward reaction rate. It should be noted that the reaction between Cs(OA) and HBr can occur at low/mild temperatures so that the $CsPbBr_3$ PNCs can be also synthesized at these low/mild temperatures, whereas the previously reported hot-injection method[1] requires high temperatures to induce the reaction between Cs(OA) and excess PbX_2.

Figures 2E–2G are TEM images of $CsPbBr_3$ PNCs produced according to the amount of added HBr. Apparently, there are no differences in the 3 samples because their sizes and shapes are the same as <10 nm and cube. However, the high-resolution TEM image in each inset indicates that some black dots exist in the $CsPbBr_3$ PNCs, and their population frequencies are greatly reduced as the HBr ratio

increases. The black dots may originate from either $PbBr_2$ formed by the incomplete reaction of (OA)$PbBr_2$(OAm) and CsBr or metallic Pb formed by the decomposition of $PbBr_2$. The metallic Pb will serve as impurities causing PL quenching. Hence, we checked the absolute PLQYs of three samples, as shown in Figure 2H. As the HBr ratio increased, the PLQY was also enhanced from 74% for 1:1 to 87% for 2:1 and 94% for the 3:1 sample. Over the 3:1 ratio, the water in the HBr solution decomposes the PNCs, so the 3:1 sample exhibited the best performance.

To confirm the tendency of PLQYs of the samples, we measured the static PL spectra of the samples with the same concentration as shown in Figure 2I. This clearly indicates that the 3:1 sample has the strongest PL intensity under the identical absorptivity. As the concentration of HBr increases, the slopes of absorption spectra were gradually steeper at near-onset absorption wavelength, and the shoulders at 495 nm became more convex. This implies that the defects of PNCs are gradually reduced with increasing HBr concentration. The corresponding transient PL decay spectra of the PNCs solutions in Figure 2J indicate that the average PL lifetimes (τ_{avg}) of the PNCs solutions gradually increase from 3.9 ns for the 1:1 to 4.4 ns for the 2:1 and to 4.6 ns for the 3:1 sample. The increased τ_{avg} may be attributed to the reduced traps in the PNCs.

The X-ray diffraction (XRD) patterns of synthesized PNCs in Figure 2K indicate that all of the samples have cubic structures and no detectable impurities such as Pb and $PbBr_2$. To check the impurities of synthesized PNCs, we measured X-ray photoelectron spectroscopy (XPS), as shown in Figure 2L. The Pb $4f_{7/2}$ and Pb $4f_{5/2}$ XPS peaks clearly indicate that the metallic Pb(0) in the PNCs is gradually decreased with increasing HBr content, and eventually the metallic Pb(0) disappears in the 3:1 sample. Accordingly, we can conclude that the PNCs prepared by the addition of a 3:1 molar ratio of HBr:$PbBr_2$ have no detectable level of $PbBr_2$ impurity by XRD and no metallic Pb(0) impurity, which causes PL quenching.

Characterization of Full-Color $CsPbX_3$ PNCs

Similar to the preparation of $CsPbBr_3$ PNCs, we synthesized full-color $CsPbX_3$ PNCs by using an HCl:HBr:HI solution with controlled molar ratio instead of an HBr solution, as shown in Table S1 and Figure 3. To prove the initiation of the reaction by the addition of HX, we checked the XRD patterns of immediately produced products by the reaction between Cs(OA) and HX (X = Cl, Br, and I) in Figure S2A. This clearly confirms the formation of CsCl, CsBr, and CsI through the reaction. The XRD patterns in Figure S2B indicate that $PbCl_2$, $PbBr_2$, and PbI_2 are also produced by the reaction between (OAm)$PbBr_2$(OA) and HX. Apparently, the formation reaction of Cs halide (CsX, X = Cl, Br, and I) by the reaction between Cs(OA) and HX was faster than the anionic exchange reaction between (OAm)$PbBr_2$(OA) and HX. Therefore, the full-color $CsPbX_3$ PNCs can be obtained by the dual role of the HX solution as reaction promoter and band gap tuner. The TEM images of full-color $CsPbX_3$ PNCs in Figures 3A–3I indicate that apparently all of the samples have similar sizes and shapes. However, the high-resolution TEM (HRTEM) image in each TEM image shows that some black dots are still in some PNCs. Figure 3J is a photograph of the full-color $CsPbX_3$ PNCs solutions (Figures 3A–3I samples) under a 365-nm UV light, which confirms that the $CsPbX_3$ PNCs can have strong PL at full-color spectrum in the visible region.

The corresponding UV-visible (UV-vis) absorption spectra and normalized PL spectra in Figure 3K and the PL spectra in Figure 3L clearly show that the emission color is tunable by controlling the molar ratio of HCl:HBr and HBr:HI. The blue (B: Figure 3A), green (G: Figure 3E), and red (R: Figure 3I) PNCs exhibited 16, 18, and 18.5 nm FWHM, respectively. Therefore, we can synthesize high-color-purity R, G, and B

CellPress
OPEN ACCESS

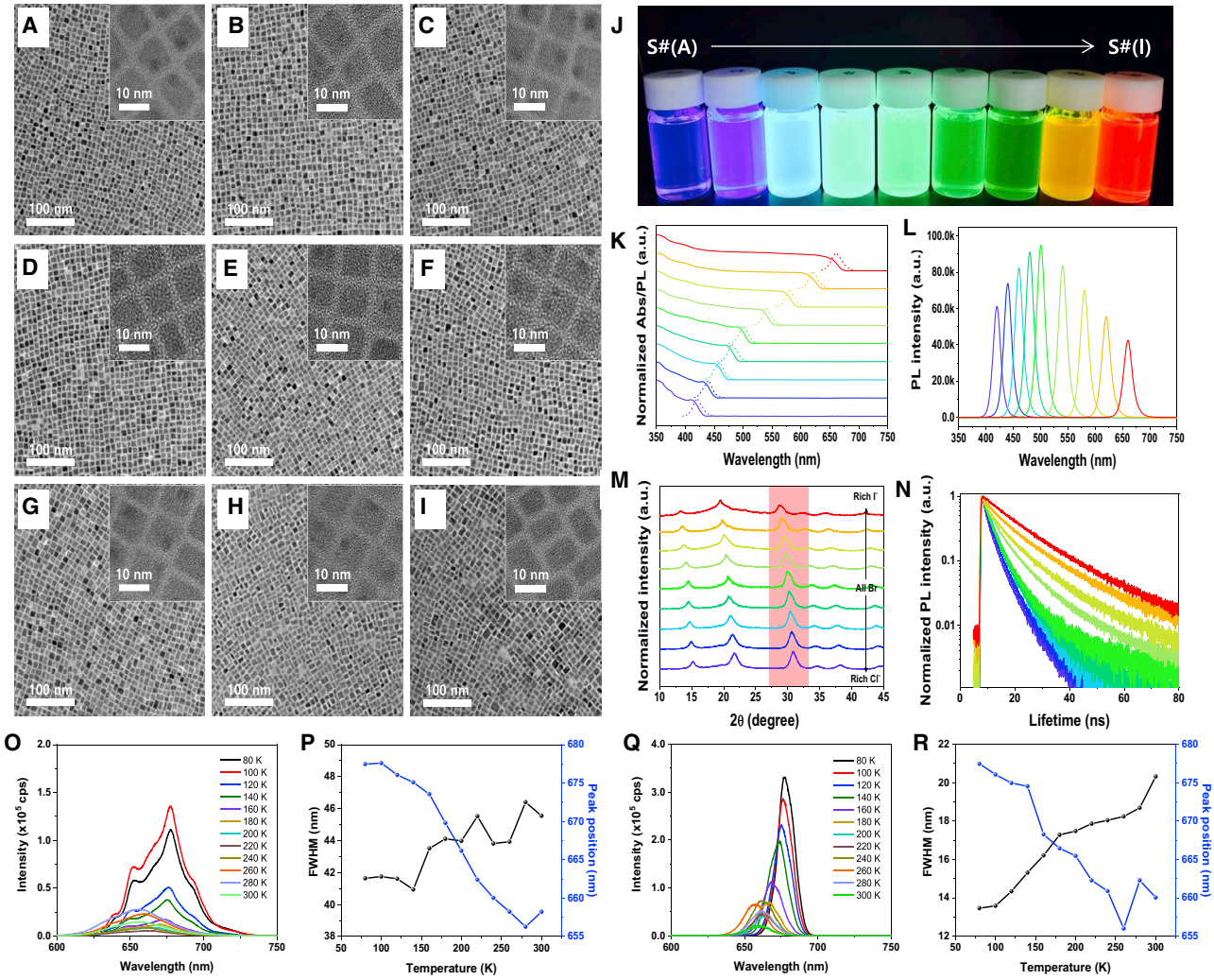

Figure 3. $CsPbX_3$ Full-Color PNCs

(A–I) TEM images of synthesized $CsPbX_3$ PNCs prepared by controlling the molar ratio of HCl:HBr and HBr:HI.

(J–N) Characterization of synthesized $CsPbX_3$ PNCs: (J) photograph of the corresponding $CsPbX_3$ solution, (K) UV-visible spectra and normalized PL spectra, (L) static PL spectra, (M) XRD patterns, and (N) transient PL decay curves.

(O–R) Low-temperature PL spectra (O and Q) and corresponding FWHMs (P and R) of I-rich $CsPbI_{3-x}Br_x$ PNCs prepared by conventional hot injection (O and P) and the new method (Q and R).

PNCs emitters with <20 nm FWHM via a new HX-mediated anionic exchange reaction. The XRD patterns in Figure 3M indicate that the Br anions in the $CsPbBr_3$ PNCs are uniformly exchanged by Cl and I anions through the reaction because all of the samples exhibit a gradual XRD peak shift and show single peaks. The transient PL decay curves in Figure 3N indicate that the τ_{avg} gradually increases from Cl-rich PNCs to I-rich PNCs because the exciton binding energies of PNCs are gradually reduced as the composition of PNCs is changed from Cl-rich to I-rich. Therefore, the reduced PL intensities of Cl-rich PNCs compared to the $CsPbBr_3$ PNCs in Figure 3L may be associated with the impurities in the Cl-rich PNCs because the Cl-rich PNCs have more black dots in the TEM images than in the others. Again, we compared the average PLQYs of 10 R, G, and B PNCs samples, as shown in Figure S3. The PLQYs of the R, G, and B samples were 73% $\pm$ 3.6% (maximum = 77%), 90% $\pm$ 2.9% (maximum = 94%), and 53% $\pm$ 3.7% (maximum = 59%), respectively.

To prove why the I-rich $CsPbI_{3-x}Br_x$ PNCs prepared by the new method have narrower FWHMs than the PNCs prepared by the conventional hot-injection method, we compared low-temperature PL spectra and corresponding FWHMs, as shown in Figures 3O–3R. At low temperature, the I-rich PNCs prepared by the conventional hot-injection method exhibited multiple PL peaks due to non-uniform halide mixing or halide anionic exchange reaction. In contrast the I-rich PNCs prepared by the new method exhibited single PL peaks, irrespective of temperature variation. This confirms that the I-rich PNCs prepared by the new method have very uniform composition by perfect anionic exchange. Therefore, it is expected that the electroluminescence (EL) devices prepared by the high-color-purity PNCs will have narrow FWHMs at full-color spectrum. Here, it should be noted that the PL intensities at low temperature are very strong and the PL intensities at room temperature are not weak because the scale of the y axis is $\times 10^5$ CPS. In general, the temperature-dependent PL spectra give more information such as exciton binding energy and interaction between electrons (excitons) and phonons (acoustic, optical, and LO [Fröhlich]).[9–11,19] However, here, we focused only on the comparison of PL spectrum-broadening phenomena according to synthetic methods.

Full-Color $CsPbX_3$ PNC-Based LEDs

Finally, we fabricated $CsPbX_3$ full-color PNC-based LEDs, as shown in Figure 4. Briefly, the $CsPbX_3$ full-color PNC-based LEDs were fabricated by sequentially depositing poly-3,4-ethylenedioxythiophene:polystyrene sulfonate (PEDOT:PSS) with tetrafluoroethylene-perfluoro-3,6-dioxa-4-methyl-7-octene-sulfonic acid copolymer (PFI), $CsPbX_3$ PNCs, 2,2′,2″-(1,3,5-benzinetriyl)-tris(1-phenyl-1-*H*-benzimidazole) (TPBI), LiF, and Al on a cleaned indium tin oxide (ITO)/glass substrate.

Table S2 summarizes the device performance of red, green, and blue $CsPbX_3$ PNC-based LEDs. Figure 4A shows current density-voltage curves of $CsPBX_3$ full-color PNC-based red, green, and blue LEDs. The turn-on voltages (luminance > 1 cd/m^2) of the red, green, and blue LEDs were ~3.4, ~3.0, and ~3.4 V, respectively. The red, green, and blue LEDs exhibited maximum luminances (L_{max}) of 1,189, 3,354, and 488 cd/m^2 (Figure 4B), maximum current efficiencies (CE_{max}) of 4.73, 39.35, and 0.77 cd/A (Figure 4C), and maximum external quantum efficiencies (EQE_{max}) of 3.06%, 10.01%, and 2.10% (Figure 4D), respectively. The normalized EL spectra of $CsPbX_3$ full-color PNC-based LEDs in Figure 4E indicate that the red, green, and blue devices exhibit the maximum EL peak position at 622, 523, and 461 nm, respectively, and have FWHMs of 26, 24, and 21 nm, respectively (see the EL spectra of another device in Figure S4). The corresponding Commission International de l'Eclairage (CIE) coordinates of each device was (0.68, 0.32) for red, (0.14, 0.77) for green, and (0.14, 0.04) for blue, respectively, as shown in Figure 4F. A summary of emission spectrum width in reported PNC-based emitters is shown in Table S3. We also checked whether the EL spectra of the R, G, and B devices change during operation.[20] The EL spectrum of the G device was slightly red-shifted to ~2 nm, whereas the EL spectra of the R and B devices were noticeably red-shifted to ~12 and ~13 nm, respectively, as shown in Figure S5.

DISCUSSION

In summary, we succeeded in synthesizing PNCs with high color purity and compositional uniformity via HX-mediated halide anion exchange at a mild temperature (~60°C). The HX triggered the reactions of Cs(OA) into CsBr and quickly produced the cube-shaped $CsPbX_3$ PNCs. During the reaction, the excess HX can be easily removed because it is a volatile gas. Consequently, the PNCs synthesized by the

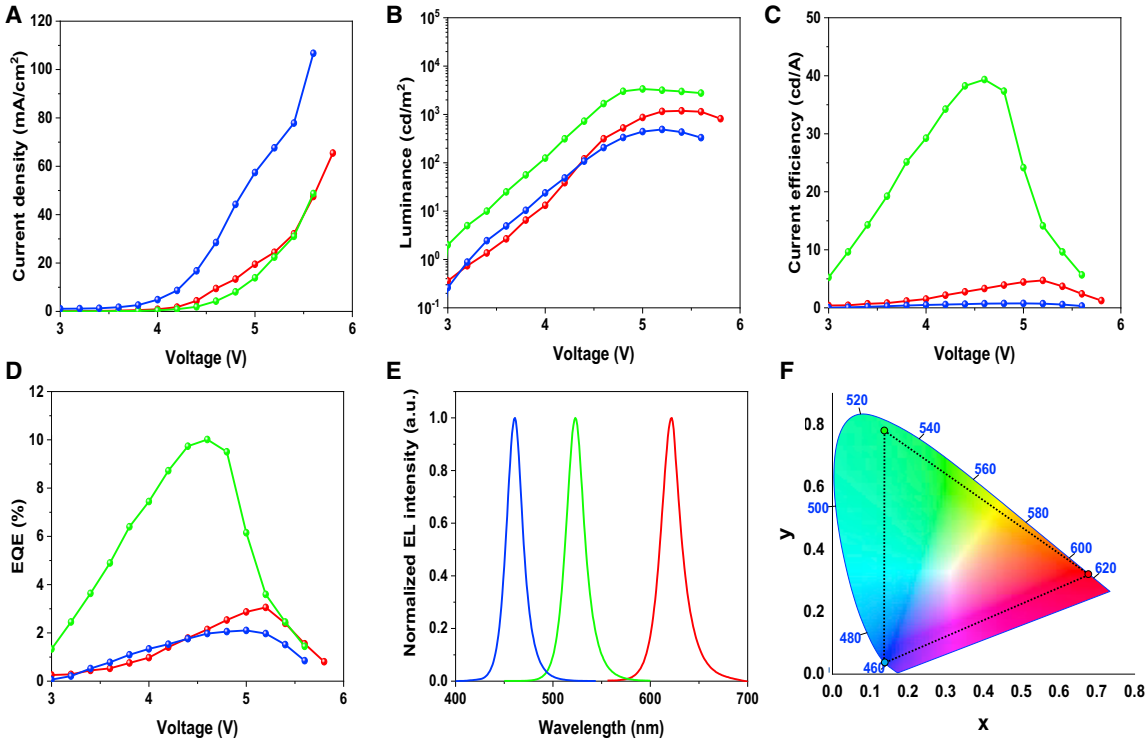

Figure 4. $CsPbX_3$ full-colored PNC-based LEDs

(A) Current density-voltage curves.

(B) Luminance-voltage curves.

(C) Current efficiency-voltage curves.

(D) External quantum efficiency (EQE)-voltage curves.

(E) Normalized EL spectra (red line = red LED, green line = green LED, and blue line = blue LED).

(F) Commission International de l'Eclairage (CIE) coordinates of PNC-based red, green, and blue LEDs.

HX-mediated method did not have metallic Pb impurities, whereas the PNCs prepared by the conventional hot-injection method had Pb/$PbBr_2$ impurities. Therefore, the PNCs prepared by the HX-mediated method exhibited high PL quantum yields. In addition, the HX reacts with $PbBr_2$ and forms $PbBr_{2-x}Cl_x$ or $PbBr_{2-x}I_x$, so compositionally uniform $CsPbBr_{3-x}Cl_x$ or $CsPbBr_{3-x}I_x$ could be obtained without mixing $PbBr_2$ and $PbCl_2$ or PbI_2. As a result, the blue, green, and red PNCs exhibited narrow emission spectra, with 16, 18, and 18.5 nm FWHMs, respectively. The low-temperature PL spectra confirmed that the HX-mediated reaction produces compositionally uniform red PNCs because the red PNCs prepared by the HX-mediated method have single peaks with narrow emission spectra, whereas the red PNCs prepared by the conventional hot-injection method have multiple peaks. Hence, the B, G, and R EL devices also exhibited narrow emission spectra.

EXPERIMENTAL PROCEDURES

Resource Availability

Lead Contact

Further information and requests for resources and reagents should be directed to and will be fulfilled by the Lead Contact, Sang Hyuk Im (imromy@korea.ac.kr).

Materials Availability

This study did not generate new unique reagents.

Data and Code Availability

All of the data associated with the studies are represented in the article and Supplemental Information. The raw data are available from the Lead Contact upon reasonable request.

Chemicals

Cs_2CO_3 (cesium carbonate, 99.9%), $PbBr_2$ (lead bromide, 98%), HI (hydriodic acid, 57 wt% in H_2O, 99.99%), HBr (hydrobromic acid, 48 wt% in H_2O, ≥99.99%), HCl (hydrochloric acid, 37 wt% in H_2O), OA (oleic acid, 90%). OAm (oleylamine, 98%), TOL (99.8%), DDAC (didodecyldimethylammonium chloride, 98%), DDAB (didodecyldimethylammonium bromide, 98%) were purchased from Sigma-Aldrich. All of the reagents were used without further purification.

Synthesis of $CsPbX_3$ PNCs

To synthesize the $CsPbX_3$ perovskite nanocrystals, we prepared Cs-oleate precursor solution by reacting Cs_2CO_3 (1 mmol, 0.326 g) and OA (3 mL) in TOL (7 mL) at 80°C until the Cs_2CO_3 powders are dissolved fully. At the same time, a $PbBr_2$-ligand precursor solution was also prepared by reacting $PbBr_2$ (2 mmol, 0.734 g) with OA (6 mL) and OAm (8 mL) in TOL (6 mL) at 80°C until $PbBr_2$ powders are dissolved fully. After cooling the 2 precursor solutions at room temperature, the $PbBr_2$-ligand precursor solution (2 mL) and TOL (20 mL) were loaded into a 70-mL vial and the vial was placed in a 60°C oil bath and stirred. As soon as stirring was started, Cs-oleate (1 mL) and aqueous HX (X = Cl, Br, I) solvent were injected in the vial containing $PbBr_2$ ligands in that order. After the HX injection, the mixture was stirred for ~10 min and the opaque solution was taken out at room temperature and cooled. To obtain pure $CsPbX_3$ perovskite nanocrystals, the opaque solution was centrifuged for 5 min at 10,000 rpm. Then, the precipitate was discarded and only the supernatant was collected. The XRD and TEM images of the precipitate in the opaque solution in Figure S6 confirmed that the precipitate was large $CsPbBr_3$ PNCs with cubic phase. The yield of the supernatant was 78%–85%. To eliminate H_2O in the HX solvent, the solvent was removed from the collected solution by using a rotary evaporator and re-dispersed in TOL. To check the effect of HBr to $PbBr_2$ in the reaction, an amount of HBr was controlled to 23, 46, and 68 μL. To synthesize the full-color CsPbX perovskite nanocrystals, we injected the controlling molar ratio of HCl:HBr:HI solvent instead of HBr alone. At this time, the total amount of HX injected was 0.6 mmol, which is 3 times the number of moles of $PbBr_2$. For HCl or HI, the amount used was 54 and 84 μL, respectively. In the combination of HCl:HBr or HBr:HI, the amounts used were calculated according to the molar ratio.

Ligand Exchange of $CsPbX_3$ PNCs Solution

A total of 100 μL OA was added in 1 mL of the red PNCs (30 mg/mL) under vigorous stirring. The mixture solution was precipitated with BuOH after centrifugation and redissolved in 2 mL octane. A total of 50 μL OA was added in 1 mL of green PNC solution (30 mg/mL) under vigorous stirring, then 100 μL DDAB TOL solution (0.05 m) were added. The mixture solution was precipitated with BuOH after centrifugation and redissolved in 2 mL octane. A total of 50 μL OA was added in 1 mL of blue PNC solution (30 mg/mL) under vigorous stirring, then 100 μL DDAC TOL solution (0.05 m) were added. The mixture solution was precipitated with BuOH after centrifugation and redissolved in 2 mL octane.

Fabrication of $CsPbX_3$ PNC-Based LEDs

Patterned ITO glass substrates (Hanalin Tech) (ITO substrate = 2.5 × 2.5 cm, etched area = 1 × 2.5 cm) were cleaned by sonication with 5% Hellmanex soap, ethanol (Samchun Chemicals), and acetone (Samchun Chemicals) for 15 min, and then shaken off the solvent using an air gun. The cleaned ITO glass substrates were treated by Ar plasma to

remove the organic residues and make the surface hydrophilic. The mixture of PEDOT:PSS (PH500, Clevios) and PFI (Sigma-Aldrich) with a specific weight ratio of 1:11 was spin coated onto the ITO glass substrate at 3,000 rpm for 60 s and annealed at 150°C for 20 min. The ligand-exchanged $CsPbX_3$ PNCs were deposited by spin coating at 1,500 rpm for 90 s in an N_2 atmosphere. A total of 50 nm TPBI (Tokyo Chemical Industry), 1 nm LiF (Sigma-Aldrich), and 50 nm Al were deposited sequentially by thermal evaporation at $<10^{-6}$ Torr. The deposition rates were 0.5, 0.1, and 2 Å/s, respectively.

Characterization

TEM images were collected on a high-resolution field emission scanning electron microsope (Tecnai 20, FEI). The *in situ* PL measurements were performed with excitation light from 365 nm UV-LEDs (M365L2, Thorlabs) delivered through optical fibers mounted to the flask during the reaction. The emission light was collected with another optical fiber. PL spectra were obtained with a spectrometer (HR2000+, Ocean Optics). UV-vis absorption spectra were measured with a UV-vis-near-infrared (NIR) spectrometer (UV-3600 Plus, Shimadzu), and PL spectra were measured with a spectrofluorophotometer (RF-6000, Shimadzu). PLQYs were measured by an absolute PL quantum yield spectrometer (C11347-11, Hamamatsu). Time-resolved photoluminescences (TRPLs) were measured using a photon-counting spectrofluorometer (ISS, pc1) under the irradiation of a 373-nm pulse laser with the excitation energy of 747 mW. XRD patterns were measured by a diffractometer (D8 Advance, Bruker) with Cu-Kα radiation at a scan rate of 5°/min. XPS spectra were measured using an X-ray photoelectron spectrometer (K-Alpha, Thermo Electron) under 1.0×10^{-8} Torr with a microfocused monochromated Al-Kα X-ray source. LED measurements were taken using a spectroradiometer (CS-2000, Minolta) and a source measurement unit (Keithley 2600).

SUPPLEMENTAL INFORMATION

Supplemental Information can be found online at https://doi.org/10.1016/j.xcrp.2020.100177.

ACKNOWLEDGMENTS

This study was supported by the National Research Foundation of Korea (NRF) under the Ministry of Science, ICT (Information and Communications Technology) and Future Planning (Basic Science Research Program, grant no. 2014R1A5A1009799) and the Nano-Material Technology Development Program (grant no. 2017M3A7B4041696).

AUTHOR CONTRIBUTIONS

J.H.H. synthesized $CsPbX_3$ PNCs and fabricated PNC-based LEDs. J.K.P. synthesized and analyzed $CsPbX_3$ PNCs. S.H.I. wrote the manuscript and supervised the work. All of the authors discussed the results and commented on the manuscript.

DECLARATION OF INTERESTS

Patent application KR10-2020-0023143 (S.H. Im, J.H. Heo, J.K. Park, Manufacturing method of perovskite compound improving color purity and perovskite optoelectronic device including the same, 2020).

Received: April 30, 2020
Revised: June 13, 2020
Accepted: July 28, 2020
Published: September 2, 2020

REFERENCES

1. Protesescu, L., Yakunin, S., Bodnarchuk, M.I., Krieg, F., Caputo, R., Hendon, C.H., Yang, R.X., Walsh, A., and Kovalenko, M.V. (2015). Nanocrystals of Cesium Lead Halide Perovskites ($CsPbX_3$, X = Cl, Br, and I): Novel Optoelectronic Materials Showing Bright Emission with Wide Color Gamut. Nano Lett. *15*, 3692–3696.

2. Tan, Z.-K., Moghaddam, R.S., Lai, M.L., Docampo, P., Higler, R., Deschler, F., Price, M., Sadhanala, A., Pazos, L.M., Credgington, D., et al. (2014). Bright light-emitting diodes based on organometal halide perovskite. Nat. Nanotechnol. *9*, 687–692.

3. Cho, H., Jeong, S.-H., Park, M.-H., Kim, Y.-H., Wolf, C., Lee, C.-L., Heo, J.H., Sadhanala, A., Myoung, N., Yoo, S., et al. (2015). Overcoming the electroluminescence efficiency limitations of perovskite light-emitting diodes. Science *350*, 1222–1225.

4. Zhang, L., Yang, X., Jiang, Q., Wang, P., Yin, Z., Zhang, X., Tan, H., Yang, Y.M., Wei, M., Sutherland, B.R., et al. (2017). Ultra-bright and highly efficient inorganic based perovskite light-emitting diodes. Nat. Commun. *8*, 15640.

5. Zou, W., Li, R., Zhang, S., Liu, Y., Wang, N., Cao, Y., Miao, Y., Xu, M., Guo, Q., Di, D., et al. (2018). Minimising efficiency roll-off in high-brightness perovskite light-emitting diodes. Nat. Commun. *9*, 608.

6. Park, M.-H., Park, J., Lee, J., So, H.S., Kim, H., Jeong, S.-H., Han, T.-H., Wolf, C., Lee, H., Yoo, S., and Lee, T.-W. (2019). Efficient perovskite light-emitting diodes using polycrystalline core-shell-mimicked nanograins. Adv. Funct. Mater. *29*, 1902017.

7. Lin, K., Xing, J., Quan, L.N., de Arquer, F.P.G., Gong, X., Lu, J., Xie, L., Zhao, W., Zhang, D., Yan, C., et al. (2018). Perovskite light-emitting diodes with external quantum efficiency exceeding 20 per cent. Nature *562*, 245–248.

8. Kim, Y.-H., Wolf, C., Kim, Y.-T., Cho, H., Kwon, W., Do, S., Sadhanala, A., Park, C.G., Rhee, S.-W., Im, S.H., et al. (2017). Highly efficient light-emitting diodes of colloidal metal-halide perovskite nanocrystals beyond quantum size. ACS Nano *11*, 6586–6593.

9. Lee, S.M., Moon, C.J., Lim, H., Lee, Y., Choi, M.Y., and Bang, J. (2017). Temperature-dependent photoluminescence of cesium lead halide perovskite quantum dots: splitting of the photoluminescence peaks of $CsPbBr_3$ and $CsPb(Br/I)_3$ quantum dots at low temperature. J. Phys. Chem. C *121*, 26054–26062.

10. Wu, K., Bera, A., Ma, C., Du, Y., Yang, Y., Li, L., and Wu, T. (2014). Temperature-dependent excitonic photoluminescence of hybrid organometal halide perovskite films. Phys. Chem. Chem. Phys. *16*, 22476–22481.

11. Cho, H., Wolf, C., Kim, J.S., Yun, H.J., Bae, J.S., Kim, H., Heo, J.-M., Ahn, S., and Lee, T.-W. (2017). High-efficiency solution-processed inorganic metal halide perovskite light-emitting diodes. Adv. Mater. *29*, 1700579.

12. Nedelcu, G., Protesescu, L., Yakunin, S., Bodnarchuk, M.I., Grotevent, M.J., and Kovalenko, M.V. (2015). Fast anion-exchange in highly luminescent nanocrystals of cesium lead halide perovskites ($CsPbX_3$, X = Cl, Br, I). Nano Lett. *15*, 5635–5640.

13. Uddin, M., Glover, J.D., Park, S.M., Pham, J.T., and Graham, K.R. (2020). Growth of highly stable and luminescent $CsPbX_3$ (X = Cl, Br, and I) nanoplates via ligand mediated anion exchange of $CsPbCl_3$ nanocubes with AlX_3. Chem. Mater. *32*, 5217–5225.

14. Lv, W., Tang, X., Li, L., Xu, L., Li, M., Chen, R., and Huang, W. (2019). Assessment for anion-exchange reaction in $CsPbX_3$ (X = Cl, Br, I) nanocrystals from bond strength of inorganic salt. J. Phys. Chem. C *123*, 24313–24320.

15. Guhrenz, C., Benad, A., Ziegler, C., Haubold, D., Gaponik, N., and Eychmüller, A. (2016). Solid-state anion exchange reactions for colour tuning of $CsPbX_3$ perovskite nanocrystals. Chem. Mater. *28*, 9033–9040.

16. Akkerman, Q.A., D'Innocenzo, V., Accornero, S., Scarpellini, A., Petrozza, A., Prato, M., and Manna, L. (2015). Tuning the optical properties of cesium lead halide perovskite nanocrystals by anion exchange reactions. J. Am. Chem. Soc. *137*, 10276–10281.

19. Wright, A.D., Verdi, C., Milot, R.L., Eperon, G.E., Pérez-Osorio, M.A., Snaith, H.J., Giustino, F., Johnston, M.B., and Herz, M.H. (2016). Electron–phonon coupling in hybrid lead halide perovskites. Nature Commun. *7*, 11755.

20. Li, G., Rivarola, F.W.R., Davis, N.J., Bai, S., Jellicoe, T.C., de la Peña, F., Hou, S., Ducati, C., Gao, F., Friend, R.H., et al. (2016). Highly efficient perovskite nanocrystal light-emitting diodes enabled by a universal crosslinking method. Adv. Mater. *28*, 3528–3534.